physica status solidi (a)

RESEARCH ARTICLE

Linking Surface Fractality and Roughness to Seebeck Response in SWCNT-Reinforced Polyester Composites

Mehmet Bayırlı[1] | Feti Gülcü[1,2] | Aykut Ilgaz[1]

[1]Department of Physics, Faculty of Science and Letter, Balıkesir University, Çagıs Kampüsü, Turkey | [2]Inebey Anatolian High School, TOKI, Yeni Mahalle, Turkey

Correspondence: Aykut Ilgaz (aykut17ilgaz@gmail.com)

Received: 11 January 2026 | **Revised:** 23 February 2026 | **Accepted:** 16 March 2026

Keywords: CNT-based polymer composites | fractal dimension | Seebeck coefficient | surface roughness | thermoelectric transport

ABSTRACT

In this study, pure polyester and 2 wt.% single-walled carbon nanotube (SWCNT)-reinforced composites were fabricated to elucidate the relationship between surface heterogeneity, fractal morphology, and thermoelectric (TE) performance. Scanning electron microscopy images were digitized and quantitatively analyzed using fractal and statistical approaches to determine fractal dimension, surface coverage ratio, cluster density, and roughness parameters. The incorporation of SWCNTs resulted in a statistically significant increase in fractal dimension from ≈1.84–1.88, accompanied by enhanced surface coverage and cluster density, indicating increased morphological complexity and network formation. Carbon nanotube (CNT) addition also led to higher surface roughness, reflecting the development of a spatially interconnected nanotube structure. TE measurements revealed positive Seebeck coefficients, confirming p-type conduction behavior. Although the Seebeck coefficient decreased with increasing electrical conductivity in the percolative regime, the power factor improved due to the dominant contribution of enhanced charge transport. These results demonstrate that CNT-induced surface heterogeneity and fractal network evolution play a decisive role in modulating electrical and thermoelectric performance in polyester-based composites.

1 | Introduction

Polyester matrix composites (PMCs) are a class of advanced materials formed by combining a polymer matrix with suitable reinforcements, resulting in tailored or synergistic properties derived from their constituents. PMCs are widely used in industrial applications such as automotive, aviation, and construction owing to their lightweight nature, high durability, cost-effectiveness, high strength, and chemical resistance. However, to achieve enhanced mechanical and thermal performance, material properties can be further improved through the incorporation of appropriate reinforcement phases. In recent years, considerable attention has been devoted to the development of composites reinforced with nanomaterials, particularly CNTs and to the investigation of their mechanical, thermal, and electrical properties. The incorporation of CNTs into polymer matrix leads to significant variations in the mechanical, electrical, and thermal behavior of the resulting composites, providing notable improvements in overall material performance [1, 2]. These enhancements are primarily associated with changes in the heterogeneous morphology of the composite system. In particular, CNT incorporation alters key structural features such as surface roughness, porosity, and fracture surface morphology.

In polyester-based polymer composites, CNTs are commonly incorporated in the form of either single-walled CNTs (SWCNTs) or multiwalled CNTs (MWCNTs). CNTs are composed of graphene sheets rolled into seamless cylindrical structures, where SWCNTs consist of a single graphene layer, while MWCNTs are formed by multiple concentric graphene cylinders [1, 3]. Owing to their one-dimensional morphology and high aspect ratio, CNTs exhibit exceptional intrinsic properties, including extremely high tensile strength, outstanding electrical conductivity, and excellent thermal stability [3, 4]. In particular, SWCNTs demonstrate high charge-carrier mobility and superior mechanical performance due to their well-defined electronic structure and the absence of interlayer interactions [3]. In contrast, MWCNTs typically provide enhanced mechanical reinforcement as a result of their multilayered architecture; however, their electrical conductivity may be relatively

lower than that of SWCNTs owing to interwall interactions and structural imperfections [4, 5].

Achieving a uniform dispersion of CNTs within a polyester matrix is essential for maximizing the associated performance enhancements. CNTs exhibit a strong tendency to agglomerate as a result of van der Waals interactions, and such aggregation can significantly deteriorate both mechanical reinforcement efficiency and the formation of effective electron transport pathways [2, 4]. To overcome these challenges, a variety of dispersion techniques—including ultrasonication, mechanical stirring, calendaring, and the use of surfactants—are commonly employed. In addition, surface functionalization strategies such as acid oxidation, covalent grafting, and polymer wrapping are widely used to improve interfacial compatibility with polyester resins and to suppress nanotube bundling, thereby promoting a more homogeneous dispersion [5].

CNT loading concentration represents another critical parameter governing the overall behavior of CNT-reinforced polyester composites. At relatively low loadings, typically in the range of ~1–2 wt.%, the composite approaches the electrical percolation threshold, leading to a rapid transition from insulating to conductive behavior [6]. The precise percolation threshold is strongly influenced by factors such as CNT aspect ratio, dispersion quality, and inters particle spacing within the polymer matrix [5, 6]. At higher CNT contents (>2 wt.%), a continuous and stable conductive network is established throughout the matrix, resulting in a substantial increase in electrical conductivity through enhanced electron tunneling and hopping mechanisms [6]. Beyond electrical performance, appropriately controlled CNT incorporation can also yield significant improvements in mechanical properties, including tensile modulus, impact resistance, and fatigue performance, provided that uniform dispersion and strong interfacial adhesion are effectively achieved [4, 5].

It is possible to infer the approximate internal structure of a material from its surface heterogeneity and morphological characteristics. One widely employed approach for quantifying surface complexity is fractal dimension analysis. In recent years, considerable research efforts have focused on using fractal-based methods to characterize the surface structures of a wide range of materials [7, 8]. The surface morphology of PMCs and CNT-reinforced PMCs is inherently heterogeneous and strongly influenced by processing conditions and CNT content. To investigate this heterogeneity, high-resolution scanning electron microscopy (SEM) is a powerful and effective characterization technique. SEM images provide detailed information about surface features and play a crucial role in the analysis and interpretation of the microstructural characteristics of composite materials. Quantitative parameters such as fractal dimension, cluster size, and surface cluster statistical distributions can be extracted from SEM images, enabling an assessment of surface complexity and structural irregularity. The fractal dimension, in particular, serves as a key descriptor of surface roughness and irregularity and is closely correlated with the mechanical and chemical properties of the material. Furthermore, particle size and cluster size distributions derived from SEM data offer valuable insights into the structure–property relationships governing the overall performance of the composites [5, 7, 9].

Numerous studies have investigated the fabrication of polyester-based composites and the evolution of their mechanical, thermal, and electrical properties upon the incorporation of carbon nanotubes (CNTs) at various loadings. Ajayan et al. reported that the mechanical properties of polyester composites, including durability, tensile strength, and elastic modulus, can be significantly enhanced through the mechanical incorporation of CNTs [1]. Similarly, Endo et al. demonstrated that precise control over the dispersion, orientation, and structural distribution of CNTs within composite systems plays a critical role in determining overall material performance [2]. In recent years, the determination of fractal dimension and cluster statistics has emerged as an effective approach for characterizing the surface morphology of nanostructured materials. Ilgaz and Bayırlı reported a clear relationship between surface morphological features and electrical conduction mechanisms in vinyl ester/CNT polymer systems. Using a combined fractal analysis and impedance spectroscopy approach, they comparatively analyzed surface microstructure and electrical conductivity behavior, revealing the presence of independent clusters with varying sizes distributed across both surface and internal regions of the composites, as observed from SEM images [5]. Consequently, fractal dimension analysis and cluster statistics are frequently employed alongside scaling theory to describe and interpret the structural characteristics of heterogeneous composite systems [2, 10, 11].

Despite these advances, studies specifically addressing the influence of CNT incorporation on the fractal characteristics of polyester-based composites remain limited. Although heterogeneous morphology analysis has gained increasing attention in materials science, particularly in relation to composite systems, only a small number of experimental investigations have examined the direct impact of heterogeneous structural features on mechanical behavior. Furthermore, the morphological characteristics and formation mechanisms associated with heterogeneous structuring in polyester composites reinforced with 2 wt.% CNTs have not yet been comprehensively explored. Polymer composites have also attracted attention as thermoelectric (TE) materials due to their low density, versatility, ease of synthesis and processing, and low thermal conductivity. The term TE is used for materials that collect wasted heat in the material and convert it into electric current. The key parameters such as thermal conductivity, Seebeck coefficient, and power factor (PF) provide information about the thermal characteristics of the material [12]. Studies on the importance of these parameters, identified with semiconductor and metal structures, in composites generally belong to recent years [13, 14]. Abd-Elsalam et al. reported the thermoelectric behavior of polyaniline-based MWCNT composites. It was found that the calculated Seebeck coefficient and PF for multiwalled CNT-reinforced composites were directly proportional to the change in temperature [13]. The maximum Seebeck coefficient and power factor obtained at 95°C reach 141 μV/K and 0.004 $\mu W/mK^2$ respectively. In the studies of Dörling et al., the Seebeck coefficient and PF were obtained as a function of electrical conductivity for CNT-added composites. It has been reported that the Seebeck coefficient is inversely proportional to the electrical conductivity, while the power factor is directly proportional to the electrical conductivity [14].

In this context, the present study aims to elucidate the relationship between heterogeneous surface morphology and the electrical and TE properties of polyester matrix composites using an integrated experimental approach. Although the effects of nanotube incorporation on the mechanical and electrical properties of polymer composites have been extensively reported in the literature, studies specifically focusing on CNT-induced variations in

surface fractal dimension, cluster distribution, surface coverage ratio, and statistical roughness parameters remain limited. Accordingly, the surface morphology of pure polyester composites and composites reinforced with 2 wt.% SWCNTs was systematically characterized using fractal analysis and scaling theory applied to high-resolution SEM images. In addition, thermoelectric parameters, including the Seebeck coefficient and PF, were evaluated to gain deeper insight into the influence of surface heterogeneity on charge-carrier transport and TE behavior. Overall, this study quantitatively demonstrates the role of nanotube incorporation in the coupled interaction between surface structure, electrical conductivity, and thermoelectric performance, thereby highlighting the potential of nanotube-reinforced polyester composites for multifunctional material design.

2 | Material and Methods

2.1 | Material

In this study, Polives 701 unsaturated polyester resin (UPR), containing 38 wt.% styrene monomer, was used as the polymer matrix. 3-Methacryloxypropyltrimethoxysilane was incorporated as a coupling agent to enhance interfacial adhesion between the reinforcement phases and the polyester matrix, thereby improving the overall mechanical performance of the composite. SWCNTs with an average diameter of ≈2 nm and a density of 1.84 g/cm^3 were supplied by OCSiAl (USA). The SWCNTs exhibited an average length of about 1.4 mm and a purity exceeding 96 wt.%. Based on these dimensions, the aspect ratio (length-to-diameter ratio) of the SWCNTs used in this study was estimated to be ≈700. Zinc sulfide was added to improve the optical and fluorescence properties of the composites and to enhance their visual appearance. Calcium carbonate was incorporated as a filler to reduce surface roughness, which can adversely affect material performance, and to improve mechanical strength. Styrene served as a reactive diluent, reducing the viscosity of the unsaturated polyester resin and thereby enhancing its processability and flow characteristics. Glass fibers with an average diameter of 12.65 μm were supplied by Şişecam (Turkey) and incorporated into the composite to enhance mechanical durability. In addition to their reinforcing capability, glass fibers offer cost-effectiveness and low moisture absorption, making them suitable for structural composite applications.

2.2 | Fractal Analysis Method

Fractal analysis was employed as an effective method to characterize surface morphology and to quantify structural heterogeneity based on observable surface features. Structural heterogeneity gives rise to localized variations in surface properties, which can be systematically evaluated using fractal and statistical scaling approaches. For this purpose, high-resolution SEM images were acquired from the surfaces of PMC and (CNT/PMC). The SEM images covered an area of 50 × 35 μm and were recorded at a resolution of 1000 × 700 pixels with 8-bit grayscale depth. To investigate regional heterogeneity, each SEM image was digitally divided into four square subregions with a side length of $L = 300$ pixels. This subregion size was selected to provide sufficient statistical representation of local surface features while maintaining sensitivity to spatial variations across the composite surface. Fractal dimension and statistical scaling analyses were subsequently performed on each region to evaluate local hetero-morphological characteristics and surface complexity. All image preprocessing and quantitative analyses were carried out using the open-source software ImageJ (version 1.53, National Institutes of Health, USA) [15, 16]. The SEM images were first converted to 8-bit grayscale format and then binarized to distinguish surface clusters from the surrounding matrix. Thresholding was performed using the IsoData autothresholding algorithm implemented in ImageJ to ensure objective and consistent segmentation across all samples. In the resulting binary images, cluster regions were defined as black pixels (binary value 0), while the matrix or void regions were defined as white pixels (binary value 255). The surface fractal dimension was determined using the standard box-counting method. In this approach, the box size (ε) was progressively reduced following a power-of-two scaling sequence, and the number of occupied boxes N(ε) was calculated at each scale. The fractal dimension (d_f) was obtained from the slope of the linear regression of log N(ε) versus log (1/ε). To ensure robustness and reproducibility, only regression fits with correlation coefficients $R^2 \geq 0.98$ were considered acceptable for fractal dimension evaluation.

3 | Results and Discussion

3.1 | Fractal Analysis

SEM observations revealed that both the pure polyester composite and the CNT-reinforced composite exhibit predominantly amorphous surface morphologies with randomly distributed surface clusters embedded within the polymer matrix. Due to the microscale resolution of the SEM images, individual CNTs at the nanoscale could not be distinctly resolved; however, elongated cylindrical features consistent with CNT bundles were observable, indicating their integration within the composite structure.

The heterogeneous nature of the surfaces is reflected in spatial variations of grayscale intensity, which correspond to differences in surface topography and cluster distribution. Darker regions are associated with recessed or lower-height areas, whereas brighter regions indicate elevated surface features. The pristine polyester composite exhibits a comparatively rougher morphology characterized by more pronounced microvoids and microcracks, likely originating from processing-induced shrinkage and interfacial stress. In contrast, the CNT-reinforced composite displays a more compact and interconnected surface structure, suggesting that CNT incorporation enhances structural integrity and reduces defect density. The comparative analysis of the four representative regions (Figures 1 and 2) highlights clear differences in spatial cluster distribution and surface coverage between the two systems. In the pure composite, cluster dispersion appears less uniform, with larger void regions interrupting surface continuity. Conversely, the CNT-reinforced sample demonstrates increased cluster connectivity and reduced inter-cluster spacing, indicative of the formation of a more continuous network structure.

The accompanying grayscale histograms further support these observations by revealing shifts in intensity distribution and pixel population density. The CNT-containing composite exhibits a more balanced intensity distribution, reflecting improved surface homogeneity and coverage. These morphological differences provide the structural basis for the variations in fractal dimension and surface coverage ratio discussed in the following sections.

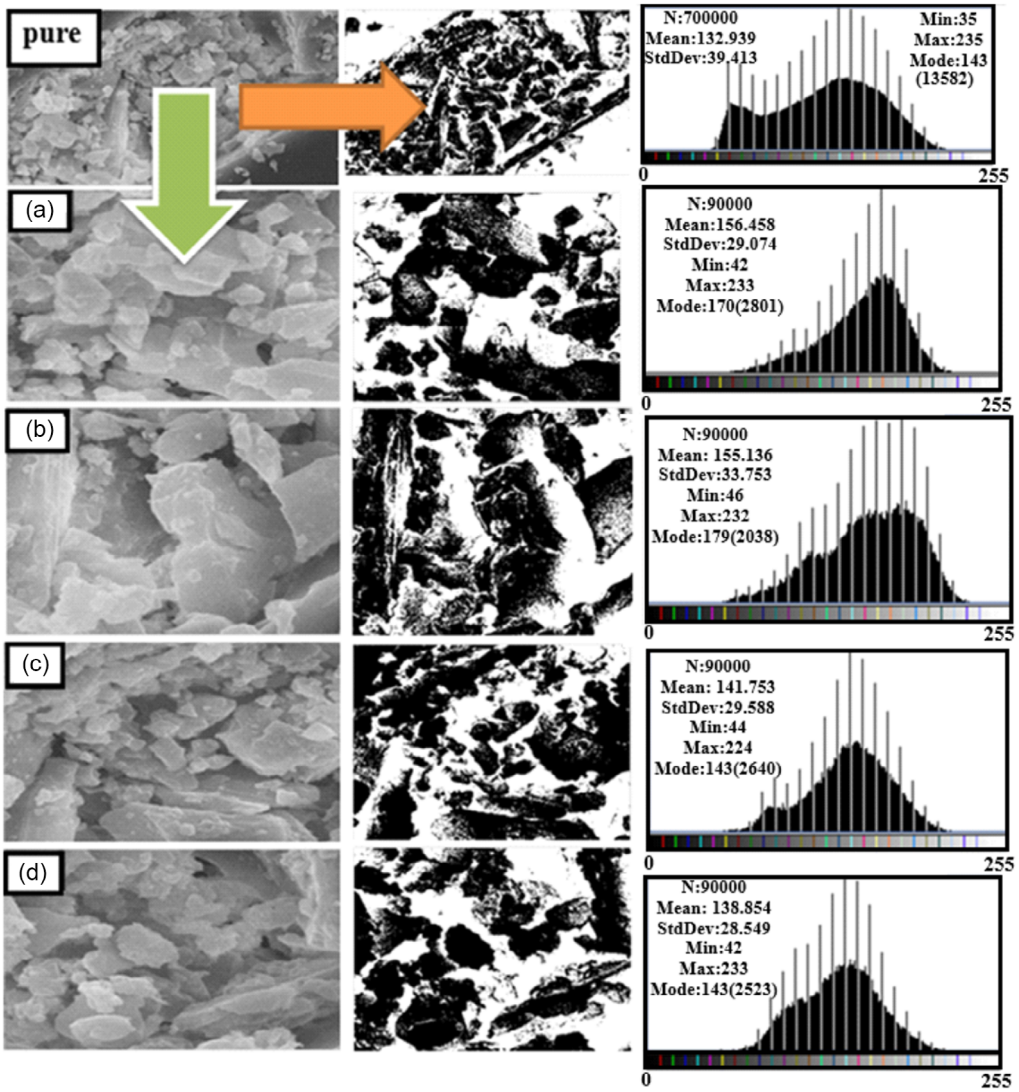

FIGURE 1 | Four different regions (a–d) taken in the SEM micro image of the pure sample without CNT doping, BMP digitized images of each and total cellular histogram diagrams for each selected region.

Figure 2 presents the corresponding SEM images, digital BMP crops, and grayscale histograms for four different regions (2a–2d) of the composite containing 2 wt.% SWCNTs. Compared to the neat sample, nanotube incorporation leads to a noticeable increase in surface coverage, accompanied by a reduction in the number of small-scale cracks and voids. These morphological changes are also reflected in the altered histogram profiles, indicating a redistribution of surface height and density features. Together, Figures 1 and 2 constitute the visual dataset used for fractal dimension and statistical scaling analyses, providing a direct comparison between the surface morphologies of the neat and CNT-doped composites. The histogram plots quantitatively represent the grayscale intensity distribution (0–255) within each selected region, where the histogram shape and peak positions reflect the relative proportions of bright (topographically higher) and dark (lower) surface areas, as well as the degree of surface homogeneity. The histograms of the pure sample (Figure 1) exhibit relatively narrower and locally separated peaks, suggesting a more heterogeneous and spatially localized variation in surface density. In contrast, the CNT/PMC (Figure 2) displays broader and more continuous histogram distributions, confirming enhanced surface coverage and increased morphological complexity induced by nanotube incorporation. These histogram characteristics are directly correlated with the calculated fractal dimension and surface statistical parameters, and they also provide insight into surface light reflectance and absorption behavior, which is closely associated with microstructural irregularities.

In addition, histograms of superficial cellular image densities for independently selected regions in the clockwise direction are also shown. Two basic concepts were defined for statistical scaling for pure and CNT reinforced sample. One of them is particle density, and the other one is surface coverage ratio. Particle density, which is the measure of the density of pixels forming the heterogeneous morphology structure, is defined as $\rho(x_i,y_j)$ for black and white pixels with x_i and y_j positions in the structure. The particle density can be defined as follows:

$$\rho(x_i,y_j)=\begin{cases}1 & \text{if dark pixels}\\ 0 & \text{else bright pixels}\end{cases} \quad (1)$$

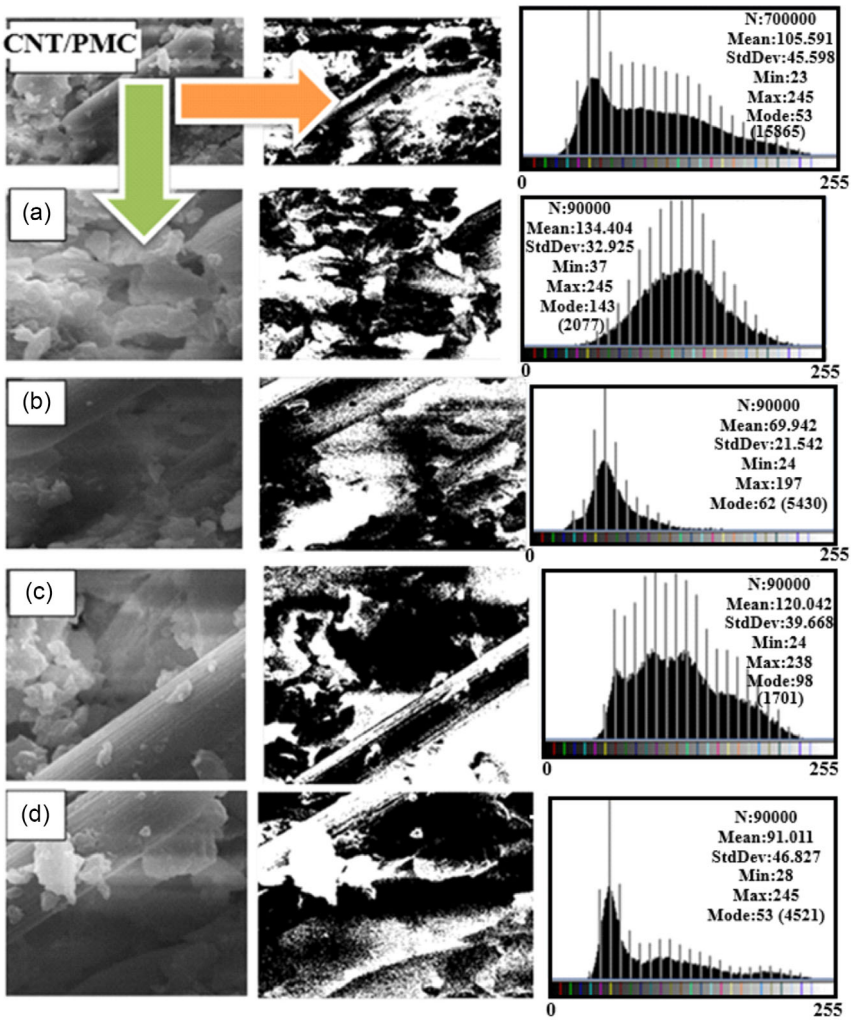

FIGURE 2 | Four different regions (a–d) taken in the SEM micro image of the CNT/PMC, BMP digitized images of each and total cellular histogram diagrams for each selected region.

where black pixels represent material components and white pixels represent the space between clusters. The surface coverage ratio determined by the probability of finding particles at the x_i and y_j positions on the lattice surface is expressed as follows [17]:

$$P(N,L) = L^{-d} \sum_{i=1,j=1}^{i=L,j=L} \rho(x_i, y_j) \tag{2}$$

where $N = \sum_{i=1,j=1}^{i=L,j=L} \rho(x_i, y_j)$ is the sum of the densities of the particles forming the heterogeneous morphology on the selected lattice surface from the sample surface and d = 2 is the Euclidean dimension. The performance of PMC and CNT/PMC composites in various applications depends not only on their chemical composition but also on the geometric complexity and morphology of their surface texture. Surface fractal morphology is characterized by scalable, self-similar features that cannot be adequately described using classical Euclidean geometry. Consequently, it plays a critical role in governing adsorption capacity and molecular diffusion behavior at the material interface, directly influencing functional performance in practical applications [18]. The complexity and degree of disorder of such surfaces are quantitatively described by the fractal dimension. Surfaces with higher fractal dimensions provide a larger number of active sites, which can enhance both electrical conductivity and interaction sensitivity. Numerous methods have been proposed to determine the fractal dimension of irregular surfaces, among which the box-counting method is one of the most widely used due to its simplicity and robustness. In the box counting method, where the fractal dimension d_f is calculated, F is a non-empty subset on the L-dimensional R^n square lattice for a CNT/PMC surface patterns, ε is the smallest possible scale (yardstick) box size, and N (ε) is the total number of these boxes. Thus, the box counting method can be applied for the smallest box size $\varepsilon \to 0$ required for the particle clusters covering the surface subset F. Accordingly, the relationship between $N(F)$ and ε can be given as follows:

$$N(F) \sim \varepsilon^{-d_f} \tag{3}$$

where d_f is the fractal dimension that determines the complexity of the pattern formed by the surface particle distribution.

The box counting dimension (K) is shown as:

$$K = \lim_{\varepsilon \to 0} \frac{N(F)}{\varepsilon^{-d_f}} \tag{4}$$

As a result, the fractal dimension (d_f) becomes:

$$d_f = \lim_{\varepsilon \to 0} \frac{\log K - \log N(F)}{\log \varepsilon} = \lim_{\varepsilon \to 0} \frac{-\log N(F)}{\log \varepsilon^{-1}} \quad (5)$$

The cluster structures observed in the SEM images of both pure and CNT-doped composite surfaces were identified through the distribution of black pixels at a given spatial scale in the binarized images, where black pixels represent clustered regions. Accordingly, the apparent cluster size on the surface is proportional to the total number of connected black pixels, which corresponds to the local surface particle density. Based on the definition of the box size in the box-counting method, the size of an individual cluster can be approximated by the number of occupied pixels n_k within a given box. In this framework, the box size ε is directly related to the pixel resolution and, therefore, to the particle density forming the surface clusters. In this study, the total particle density value of the clusters forming the surface was calculated by grouping according to the N (ε) [$\varepsilon = 2^i$ (i = 1, 2, …, n)] binary number system as shown in Figures 3 and 4 for pure and doped specimen, respectively. After the linearly obtained dataset is transferred to the graph on logarithmic axes, the fractal dimension (d_f) is calculated from the slope of the regression line obtained. The fractal dimension $d_f \in Q$ is determined as a rational number and takes values between $1 \leq d_f \leq 2$. Thus, the fractal dimension relation in the box counting method can be defined as follows:

$$\log N(\varepsilon) = -d_f \log(\varepsilon) + C \quad (6)$$

While the slopes of the $\log N(\varepsilon)$ and $\log(\varepsilon)$ graphs for the fractal dimension were determined by the linear regression method, the $p < 0.001$ results, which generally test the hypothesis that the independent variable has no effect on the model and its coefficient is zero, were taken as basis. For the undoped sample, the coverage ratio values vary between 53.754% and 59.529%, while the fractal dimensions vary between 1.824 and 1.854. For the undoped polyester composite, the surface coverage ratio ranged from 53.754% to 59.529%, while the corresponding fractal dimension values varied between 1.824 and 1.854. In contrast, the CNT/PMC exhibited higher coverage ratios, ranging from 58.091% to

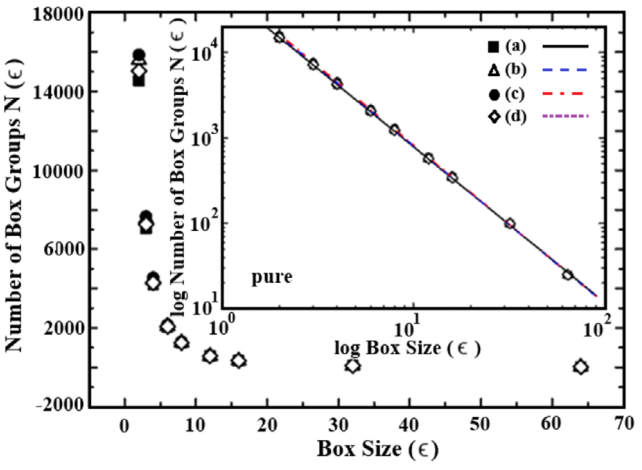

FIGURE 3 | Distribution of the particle density of four different regions selected from the pure composite surface according to the number of particle groups in the selected box size. Logarithmic values and linear regression lines are shown in the inset graph.

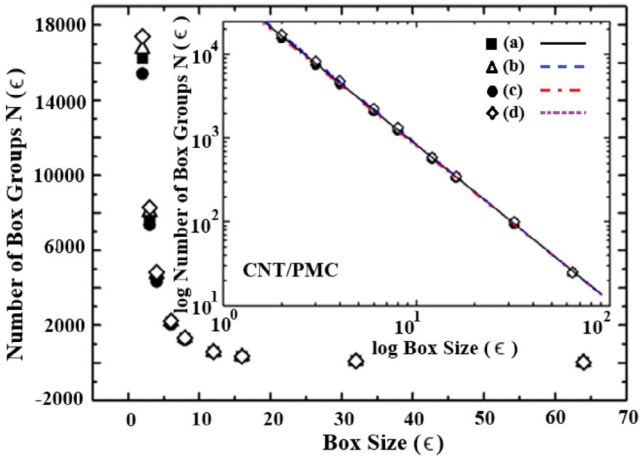

FIGURE 4 | Distribution of particle density of four different regions selected from carbon nanotube doped composite surface according to the number of particle groups in the selected box size. Logarithmic values and linear regression lines are shown in the inset graph.

63.638%, accompanied by an increase in fractal dimension from 1.853 to 1.885. The systematic increase in fractal dimension with increasing surface coverage indicates that CNT incorporation effectively fills surface cracks and voids, leading to a more complex and space-filling surface morphology. This trend is also clearly observed in the digitized bitmap representations derived from the SEM images, where CNT/PMC displays a more continuous and homogeneous cluster distribution compared to the undoped material. Consistent with these observations, Zhang et al. reported that fractal dimension values—used as an indicator of CNT-induced void-filling efficiency in doped composites produced by different fabrication techniques can be reliably estimated from SEM image analysis [17].

Pander et al. investigated the fractal characteristics of CNT-reinforced composites and reported fractal dimension values ranging from 1.75 to 1.88 [9]. Similarly, Ilgaz and Bayırlı found that the fractal dimension varied between 1.737 and 1.790 for neat composites and increased to the range of 1.757–1.817 for single-walled carbon nanotube (SWCNT)-reinforced systems [5]. These studies consistently demonstrate that CNT incorporation leads to higher surface coverage and increased fractal dimension compared to unfilled composites. Accordingly, the addition of an appropriate amount of CNTs effectively reduces large-scale cracks and voids in the heterogeneous surface structure, thereby contributing to improved mechanical integrity and enhanced electrical performance. In addition to fractal dimension, cluster statistics were also evaluated in the present study. For the pure polyester composite, the number of clusters varied regionally between 389 and 473, resulting in a total cluster count of 2705. Upon CNT incorporation, the regional cluster numbers increased and ranged between 492 and 857, with a total of 4673 clusters. This corresponds to an ≈73% increase in total cluster count, indicating a significant enhancement in surface heterogeneity induced by nanotube addition.

This marked increase in cluster count provides indirect yet valuable insight into the CNT dispersion state. The transition from fewer, larger clusters in the neat sample to a higher number of smaller clusters in the CNT/PMC suggests that the nanotubes are not uniformly dispersed at the molecular level, but instead

form a spatially interconnected network of finely distributed agglomerates. Such behavior is consistent with the intrinsic tendency of CNTs to bundle due to strong van der Waals interactions between adjacent nanotubes [2, 4]. Importantly, the regional variation in cluster numbers—ranging from 492 to 857 across different sub regions of the same CNT-doped sample—indicates heterogeneous dispersion quality, where certain areas contain denser CNT-rich domains than others. Regions with higher cluster density (e.g., Region 2b with 857 clusters) are expected to facilitate enhanced local connectivity and reduced inter-tube tunneling distances, thereby promoting conductive pathway formation, whereas regions with lower cluster density may act as transport-limited zones. Therefore, the overall electrical response of the composite is governed not only by CNT loading but by the statistical distribution and connectivity of CNT-rich and CNT-poor domains, reflecting a percolative transport mechanism.

The observed increase in cluster number does not contradict the void-filling effect of CNTs; rather, it suggests a transition from fewer large-scale defects to a higher number of smaller and more uniformly distributed surface features. This interpretation is further supported by the summarized fractal dimensions, regression constants, and cluster statistics as a function of surface coverage ratio presented in Table 1. A similar increase in cluster density for CNT/PMC was also reported by Ilgaz and Bayırlı, where it was correlated with changes in electrical conductivity behavior [5]. Pander et al. additionally demonstrated that high cluster density in CNT forests leads to increased surface area and enhanced adsorption capacity [9]. Although the material systems differ, this finding supports the notion that increased cluster density can improve functional surface properties. Nevertheless, the intrinsic tendency of CNTs to agglomerate must be carefully considered, as excessive agglomeration can increase surface roughness and adversely affect electrical conductivity [19, 20]. Therefore, the increase in cluster number should be evaluated in conjunction with the homogeneity of CNT dispersion to achieve optimal composite performance.

From a charge transport perspective, the simultaneous increase in fractal dimension and cluster density indicates the development of a more spatially interconnected CNT network within the polyester matrix. A higher fractal dimension reflects enhanced geometrical complexity and a greater probability of inter-cluster connectivity, effectively reducing the average tunneling distance between neighboring nanotubes. As the network approaches the percolation threshold, carrier hopping across CNT junctions becomes more efficient, resulting in the establishment of continuous conductive pathways. Thus, the observed morphological evolution is not merely a surface topography modification but corresponds to a fundamental restructuring of the internal charge transport network.

Standard deviation values for each regional measurement are explicitly reported in Table 1 (e.g., 1.824 ± 0.012 for Region 1a), providing a quantitative measure of variability in the fractal dimension calculations across subregions. The average fractal dimensions, presented together with their overall standard deviations (1.841 ± 0.013 for the neat sample and 1.869 ± 0.014 for the CNT-doped sample), indicate a clear and reproducible increase upon CNT incorporation. Statistical comparison between the neat and CNT/PMC was performed using an independent two-sample t-test (n = 4 per group), and the difference in fractal dimension was found to be statistically significant ($p = 0.026$). In addition, the overall measurement uncertainty associated with the image-based fractal analysis procedure was estimated to be ≈1%, based on repeated calculations under identical processing parameters.

3.2 | Determination of Statistical Roughness Quantities

In this part of the study, statistical descriptors of surface heterogeneity were calculated using SEM images in combination with Gwyddion software. Fundamental parameters describing the surface height distribution—namely variance, skewness, and kurtosis

TABLE 1 | Estimated morphological parameters for composite structures samples.

Sample	Region	Coverage Ratio (%)	Fractal dimension (d_f)	Regression coefficient (R^2)	Cluster number (n)
Neat (PMC)	Whole sample	50.527	1.859 ± 0.008	0.99993	2705
	(a)	53.754	1.824 ± 0.012	0.99984	473
	(b)	56.031	1.848 ± 0.010	0.9999	471
	(c)	59.529	1.854 ± 0.011	0.99987	389
	(d)	56.279	1.837 ± 0.011	0.99988	429
	Average	56.398	1.841 ± 0.013	—	—
CNT doped (CNT/PMC)	Whole sample	58.128	1.879 ± 0.009	0.99991	4673
	(a)	60.223	1.862 ± 0.008	0.99993	510
	(b)	58.377	1.874 ± 0.009	0.99993	857
	(c)	58.091	1.853 ± 0.004	0.99998	492
	(d)	63.638	1.885 ± 0.008	0.99993	685
	Average	60.082	1.869 ± 0.014	—	—

were determined from rectangular regions with dimensions of $50 \times 35\,\mu m$, and the corresponding results are summarized in Table 2. Structural surface roughness analysis enables the identification of micro- and macro-scale surface defects, fluctuations, and irregularities originating from the fabrication process. When carbon nanotubes are incorporated into composite materials, they can significantly alter surface characteristics, particularly surface roughness. Depending on the CNT loading level and dispersion quality, nanotube incorporation may lead to either surface smoothing or increased roughness. Consequently, the spatial distribution of CNTs within the matrix and the resulting morphological evolution of the surface are closely related to nanotube orientation and local cellular density. Surface roughness is commonly defined as the deviation of surface height values relative to a reference plane. It can be evaluated along a single direction, along a selected reference line, or over multiple parallel scan directions. In general, SEM image data can be represented as a two-dimensional discrete data space of size $L \times M$, where L and M denote the number of rows and columns, respectively. The corresponding physical lattice area is defined as $L_x \times M_y$ for L and M, where L_x and M_y are the dimensions along the axes of the restricted area. The horizontal distance between two adjacent scan points is defined as the sampling interval and denoted by ΔL_x. The determination of the cellular image height value on the surface of the sample can be determined by the total cellular image height values in certain regions in addition to the change in both horizontal and vertical directions with respect to the 2D reference line. Therefore, the determination of statistical quantities can be performed with an arbitrary $\xi(x, y)$ image density function. In general, $\xi(x, y)$ is used as an n-order polynomial function.

The roughness parameter for the sample surface is a natural measure of the deviations of the cellular values in the sampling area on the image surface from the average reference plane. The mean square roughness or root mean square (*rms*) value R_A of the height irregularities can be determined by reference to the 2nd central moment of the statistical data values. The standard deviation σ of the cellular image intensities is the square root of the arithmetic mean of the square of the vertical deviation from the mean line across the limited image grid. Therefore, the statistical moment of the values is defined by the following relationship:

$$m_i = \left(\left(L^{-d}\right) \sum_{i=0,j=0}^{L_{max}} \left(z_{i,j} - \overline{z}\right) \right)^i \tag{7}$$

where L is the sampling length of the image, $d = 2$ is Euclidean dimension value, $\overline{z}$ is the surface image flux density obtained by dividing it by the surface mesh area. The surface image density is defined as follows:

$$\overline{z}(h, L) = \left(L^{-d}\right) \sum_{i=1,j=1}^{L_{max}} z_{i,j} \tag{8}$$

where $\sum_{i,j}^{L} z_{i,j}$ is the sum of the image intensities of pixels located at $x_i < L_{max}, y_j < L_{max}$ on the surface of the material displayed in grayscale TIFF format. These values are calculated by taking the total number of pixels forming different clusters and cluster groups on the surface as reference. Also, $z_{i,j}$ is the height value at each cellular data point according to the grayscale scale in the 3D image of the brightness and darkness of the pixels. L is the lateral length value of the closed mesh bounded by the image. The height value for each pixel of the cellular change array in the sample surface image is defined by the following relationship:

$$z_{i,j} = \begin{Bmatrix} 0 & \text{dark color} \\ \text{from 0 to 255} & \text{bright color} \end{Bmatrix} \tag{9}$$

In the statistical moment equation in Equation (7), $m_1 = 0$ is obtained for $i = 1$. The variance value determining the roughness can be calculated from the 2nd central moment of the total data values of the mean square roughness or the *rms* of the height irregularities. The statistical 2nd moment of the data distribution is given as follows:

$$\sigma = m_i^{1/2} \tag{10}$$

where σ is the standard deviation, represented by R_A and is the square root of the arithmetic average. Vertical deviation from a reference line is expressed as:

$$R_A = rms = \left(\left(L^{-d}\right) \sum_{i=0,j=0}^{L_{max}} \left(z_{i,j} - \overline{z}\right) \right)^k \tag{11}$$

If the k exponent in the equation is 1/2, the surface roughness determines the *rms* value. For surfaces with a Gaussian distribution, the normalized form of the distortion is the statistical 1st moment. The 1st moment can be written as:

$$m_1 = S_A = \frac{1}{\sigma^3 L} \sum_{i=1,j=1}^{L_{max}} \left(z_{i,j} - \overline{z}\right)^3 \tag{12}$$

Kurtosis can be calculated as the statistical second moment as follows:

$$m_2 = K = \frac{1}{\sigma^3 L} \sum_{i=1,j=1}^{L_{max}} \left(z_{i,j} - \overline{z}\right)^4 \tag{13}$$

TABLE 2 | Statistical parameters of surface heterogeneous morphology for PMC and CNT/PMC.

Statistical parameters	PMC	CNT/PMC
	Moment based	
Mean value ($\overline{z_{i,j}}$ μm)	33.76	27.02
Roughness (*rms*) (R_A μm)	10.07	11.68
Main Roughness (S_A nm)	8.44	9.82
Skew (S_k μ*m*)	−0.1838	0.5310
Kurtosis (K)	−0.9006	−0.6098
	Order based (μm)	
Minimum	8.92	5.86
Maximum	59.92	62.47
Median	34.93	25.50
Maximum peak height (S_p)	26.17	35.45
Maximum pit depth (S_v)	24.83	52.116
Maximum height (S_z)	51.00	56.61

The incorporation of CNTs into pristine polymer composites is expected to significantly influence both the internal structure and the surface morphology of the material. In particular, non-uniform dispersion of CNTs stemming from their intrinsic tendency to agglomerate—can lead to pronounced variations in surface roughness. To quantitatively assess this effect, the SEM images were discretized onto an $L \times M$ mesh, and surface roughness parameters were calculated based on the cellular image density z_i evaluated over the sampling interval ΔL. The grayscale-based cellular image density values were found to vary between 0 and 255, corresponding to the minimum and maximum surface height contrasts, respectively. Figure 5a,b illustrates the spatial variation of cellular image density for the pure and doped samples along the L-direction of the lattice. Comparative analysis reveals that, although the surface of the pure composite exhibits strong fluctuations and irregular variations, the CNT/PMC shows a clear tendency toward a more regular and stabilized surface profile. Owing to the random selection of the analyzed surface region, the CNT-doped sample displays regional variations in nanotube distribution. Accordingly, two distinct fluctuation regimes can be identified for the doped composite. In regions with higher nanotube density, the cellular image density exhibits smoother and more regular variations, particularly for spatial scales below $L < 1$ μm. This behavior indicates that, despite the overall heterogeneous dispersion of CNTs, nanotube incorporation promotes a transition toward a more ordered surface morphology by reducing large-amplitude height fluctuations and stabilizing local surface features.

When Table 2 is examined, the average surface height is observed to decrease from 33.76 to 27.02 μm following CNT incorporation. This reduction suggests that nanotube addition contributes to partial filling of surface voids and local densification of the polymer matrix, leading to a more compact surface structure. At the same time, the roughness parameters provide further evidence of CNT agglomeration and heterogeneous dispersion. Although certain surface regions become densified, the overall average roughness (R_a) increases from 10.07 to 11.68 μm, indicating the emergence of additional micro-scale irregularities associated with CNT-rich domains. The substantial increase in maximum pit depth (S_v) from 24.83 to 52.116 μm is particularly revealing. This pronounced rise indicates the formation of deep surface depressions that can be attributed to CNT agglomeration.

During curing, densely bundled nanotube regions may experience differential shrinkage or localized interfacial stress, leading to partial detachment from the surrounding polymer matrix and the formation of pits or voids at agglomerate boundaries. Concurrently, the increase in maximum peak height (S_p) from 26.17 to 35.45 μm suggests the presence of protruding CNT-rich domains extending above the matrix surface. The transition of the skewness parameter from a negative value (−0.1838) for the neat composite to a positive value (0.5310) for the CNT-reinforced sample is particularly significant. A positive skewness indicates that the surface morphology becomes dominated by sharp peaks rather than deep valleys, implying that CNT agglomerates now represent the primary surface features instead of the voids and cracks observed in the unfilled composite. The increase in kurtosis (from −0.9006 to −0.6098) further suggests a more concentrated height distribution, reflecting the coexistence of pronounced peaks and localized depressions.

The spatial variation in CNT distribution is also evident in Figure 5b, which reveals two distinct fluctuation regimes. At smaller spatial scales ($L < 1$ μm), the surface exhibits smoother and more regular image-density variations, indicating that in well-dispersed micro-domains CNTs effectively fill nanoscale irregularities and stabilize local morphology. However, this nanoscale regularization coexists with microscale agglomeration-induced roughness, demonstrating a scale-dependent influence of CNT incorporation. This dual nature of CNT distribution—simultaneously filling voids at the nanoscale while forming agglomerates at the microscale—represents a key structural finding. The dispersion quality is therefore not uniform but bimodal, consisting of well-dispersed CNT regions that enhance local densification and agglomerated regions that introduce structural heterogeneity. From a transport perspective, this morphology implies that electrical conduction occurs through a statistically distributed percolation network, where both individual nanotubes and small agglomerates contribute to pathway formation. In this framework, CNT-rich agglomerates may function simultaneously as conductive nodes and localized scattering centers, thereby influencing both electrical conductivity and TE response.

Overall, CNT incorporation significantly modifies the morphometric statistics of the polyester composite surface, including roughness (R_a), skewness (S_k), kurtosis (K), and extreme height parameters (S_v and S_p). A comparative examination of Tables 1 and 2 further reveals that fractal dimension and roughness trends are not strictly parallel. While the fractal dimension increases, indicating enhanced spatial complexity and connectivity, the average surface height decreases, reflecting local densification. This demonstrates that CNTs simultaneously fill certain surface regions while locally amplifying height variations in others,

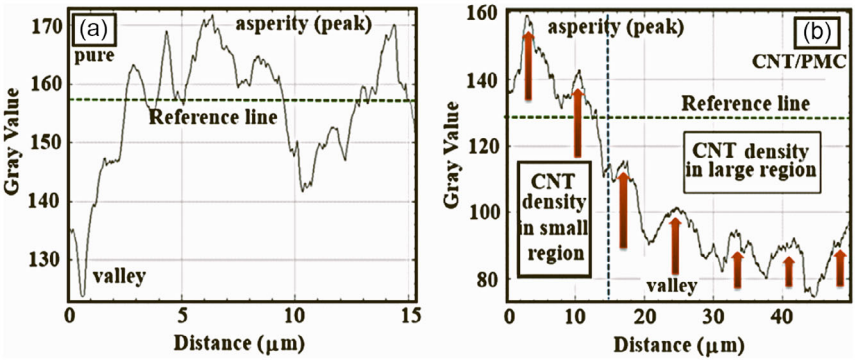

FIGURE 5 | Cellular image density variation in the L-dimensional lattice of (a) pure and (b) CNT-doped sample surfaces.

resulting in a more space-filling yet statistically complex surface morphology. Such a tunable balance between surface complexity and roughness is particularly advantageous for applications requiring optimized interfacial properties, including energy storage systems, gas-sensing devices, and dielectric materials, where controlled surface morphology plays a critical role in performance and reliability.

As reflected by the statistical moment–based parameters summarized in Table 2, CNT incorporation leads to a decrease in the average image intensity and kurtosis, while simultaneously increasing the surface roughness, average roughness, and curvature-related parameters. These results clearly indicate that nanotube doping induces a more heterogeneous surface morphology characterized by enhanced height fluctuations and localized surface features. The observed increase in surface roughness is a particularly important outcome for applications such as micro-capacitors and energy storage devices. In supercapacitor electrodes, for example, higher surface roughness is often desirable because it increases the effective surface area available for charge accumulation, thereby enabling higher energy storage capacity [21]. However, excessively rough surfaces can also lead to undesirable effects. Increased roughness may cause local electric field intensification and field concentration at sharp surface features, which can elevate the risk of dielectric breakdown. Such effects can adversely impact capacitance stability and reduce device lifetime. In contrast, for gas and biosensing applications, rough and heterogeneous surfaces are generally advantageous, as they provide a greater number of active binding sites for target molecules and enhance detection sensitivity. Therefore, the surface roughness induced by CNT incorporation must be carefully optimized according to the specific functional requirements of the intended application.

3.3 | Thermal Characterization

The theory of thermoelectric energy conversion is based on the coupled transport of charge carriers and entropy within a material. When a TE material is subjected to a local temperature gradient (∇T) and a gradient in the electrochemical potential of the charge carriers $\left(\nabla \frac{\tilde{\mu}}{q}\right)$, the resulting local flux densities of charge (j_q) and entropy (j_s) can be expressed within the framework of linear irreversible thermodynamics as follows [22]:

$$\begin{pmatrix} j_q \\ j_s \end{pmatrix} = \begin{pmatrix} \sigma & \sigma.S \\ \sigma.S & \sigma.S^2 + \Lambda \end{pmatrix} . \begin{pmatrix} -\nabla \frac{\tilde{\mu}}{q} \\ -\nabla T \end{pmatrix} \tag{14}$$

The thermoelectric tensor is represented by the following three parameters: σ is the isothermal electrical conductivity, S is the Seebeck coefficient, Λ is the open-circuit entropy conductivity. When CNTs, which possess intrinsically high electrical conductivity, are incorporated into polymer matrices that are otherwise electrically insulating, the electrical conductivity of the composite can be significantly enhanced while maintaining relatively low thermal conductivity. Although low thermal conductivity may generally limit TE performance, the presence of nanofillers can partially compensate for this effect by modifying phonon scattering mechanisms, thereby mitigating excessive heat transport [13]. This interplay also influences the Seebeck coefficient (S). While S is macroscopically defined as the thermoelectric voltage generated per unit temperature difference, it corresponds microscopically to the entropy transported per unit charge carrier [13].

Under an applied temperature gradient, charge carriers on the hotter side of the material possess a higher average thermal velocity. These faster carriers transport entropy toward the colder region, giving rise to a TE voltage. A quantitative description of this phenomenon can be derived from the Bethe–Sommerfeld expansion, yielding the following expression for the Seebeck coefficient:

$$S = \frac{\pi^2 k_B}{3e}(k_B T)\left[\frac{1}{n(E)}\frac{\mathrm{dn}(E)}{\mathrm{dE}} + \frac{1}{\mu(E)}\frac{\mathrm{d}\mu(E)}{\mathrm{dE}}\right] \tag{15}$$

where k_B is Boltzmann's constant, e is the electron charge, T is absolute temperature, $n(E)$ is carrier density, $\mu(E)$ is mobility. The Seebeck coefficient is a key parameter in the dimensionless thermoelectric figure of merit ZT, which is widely used to evaluate the overall performance of TE materials by simultaneously accounting for electrical conductivity, thermal conductivity, and thermopower. It is defined as

$$\mathrm{ZT} = \frac{S^2 \sigma T}{\lambda} \tag{16}$$

where σ and λ are electrical and thermal conductivity, respectively. In this study, the Seebeck coefficient, also referred to as thermopower, was experimentally determined by positioning the samples between two temperature-controlled blocks. The temperatures at the hot and cold sides were measured directly from the sample surface using a calibrated thermocouple, ensuring accurate determination of the temperature gradient across the specimen. According to Equation (16), the term $S^2\sigma$ is defined as the PF, which is a key parameter for evaluating thermoelectric performance independent of thermal conductivity [13].

The variation of the Seebeck coefficient as a function of electrical conductivity, including standard deviation error bars obtained from repeated measurements, is presented in Figure 6. As observed, the Seebeck coefficient of the CNT/PMC composites systematically decreases with increasing electrical conductivity. The relatively small error bars indicate good experimental

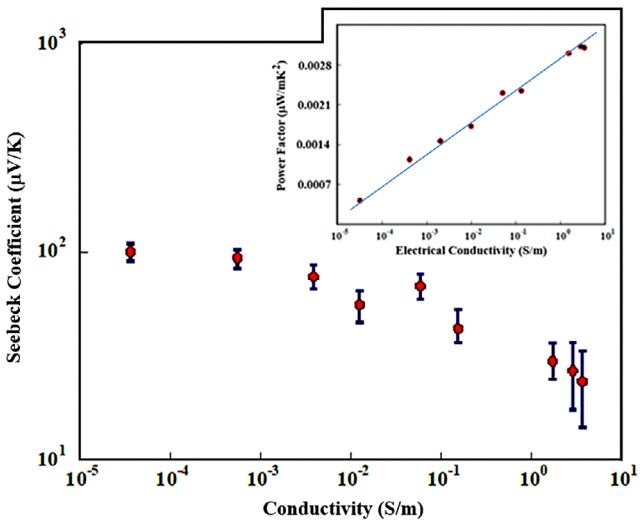

FIGURE 6 | Seebeck coefficients CNT/PMC as a function of their electrical conductivity.

reproducibility and confirm the robustness of the inverse trend. This behavior can be interpreted in the context of the fractal CNT network structure discussed above. The increased junction density associated with higher fractal dimension introduces additional CNT–CNT and CNT–polymer interfaces that act as localized potential barriers within the composite. These heterogeneous interfaces promote energy-dependent carrier scattering, selectively influencing carriers near the Fermi level. According to the Mott relation, the Seebeck coefficient depends on the energy derivative of electrical conductivity; therefore, morphology-induced modifications of carrier concentration and mobility directly affect thermopower. While enhanced percolation increases carrier concentration and electrical conductivity, the simultaneous presence of interfacial barriers modulates carrier energy distribution, resulting in the observed decrease in Seebeck coefficient.

This inverse conductivity–thermopower relationship is well established in TE systems and primarily arises from the increase in carrier concentration and the formation of more efficient charge transport pathways induced by CNT incorporation. All measured Seebeck coefficients remain positive, indicating hole-dominated (p-type) conduction. This observation is consistent with previously reported CNT-based polymer composites, where oxygen adsorption and the intrinsic electronic structure of CNTs promote p-type transport behavior. The inset plot corresponds to a Type-I Ioffe representation, in which the PF ($S^2\sigma$) is plotted as a function of electrical conductivity to evaluate the trade-off between thermopower and charge transport efficiency. As shown, the power factor increases nearly proportionally with electrical conductivity, reflecting the dominant contribution of improved charge transport to the overall thermoelectric response. Despite the relatively low CNT loading, the obtained PF values are comparable to those reported for polymer-based TE composites, demonstrating that controlled CNT-induced network formation effectively enhances thermoelectric performance without compromising structural lightweight characteristics.

The findings of this study clearly demonstrate a strong correlation between surface morphology and the electrical as well as TE properties of the composites. Fractal analysis revealed that the fractal dimension of the pure polyester composite ranged from 1.824 to 1.854, whereas this value increased to 1.853–1.885 upon the incorporation of 2 wt.% SWCNTs, indicating a pronounced enhancement of morphological heterogeneity induced by the nanotubes. In parallel, the coverage ratio increased from 53.754 to 59.529% in the pristine sample to 58.091–63.638% in the CNT-doped composite, confirming that the nanotubes effectively fill surface voids and expand the interconnected conductive network. These observations are in good agreement with the findings of Ilgaz and Bayırlı, who reported that an increase in fractal dimension in CNT-based composites leads to enhanced electrical conductivity. Similarly, Pander et al. reported fractal dimension values ranging between 1.75 and 1.88 for CNT forests, demonstrating that the values obtained in the present study are fully consistent with those reported in the literature. Surface roughness analysis further supports the morphological evolution induced by CNT addition. While the average surface height decreased from 33.76 to 27.02 μm, the arithmetic mean roughness (R_A) increased from 10.07 to 11.68 μm, suggesting that CNT incorporation results in a more compact structure accompanied by increased micro-scale surface irregularities. Moreover, the transition of the skewness parameter from −0.1838 to +0.5310, together with the increase in maximum valley depth (S_v) from 24.83 to 52.116 μm, indicates the formation of localized CNT agglomeration regions. Electrical and thermoelectric measurements exhibited trends that are fully consistent with the observed surface morphology. The positive Seebeck coefficient confirms the p-type conduction behavior of the composites, while the increase in power factor, driven primarily by enhanced electrical conductivity, follows the trend reported by Dörling et al. for CNT-doped polymer systems. Overall, increasing the fractal dimension from ≈1.84–1.88 not only enhances surface complexity but also significantly improves electrical conductivity and TE performance, highlighting the critical role of the CNT-induced percolation network in strengthening both the structural and functional properties of the composite.

4 | Conclusion

In this study, the surface heterogeneity of polymer composites incorporating 2 wt.% CNTs was systematically investigated using fractal analysis and higher-order statistical surface descriptors. CNT incorporation led to a measurable increase in surface fractal dimension, reflecting enhanced geometrical complexity and the development of a spatially interconnected CNT-mediated network. Statistical image-density and roughness analyses confirmed that nanotube dispersion governs surface coverage, junction density, and local heterogeneity, establishing a clear structural basis for transport modulation.

The results reveal a scale-dependent morphological evolution in which nanoscale void filling coexists with microscale CNT agglomeration. This bimodal dispersion behavior promotes the formation of an effective percolation network while simultaneously introducing localized heterogeneity. The increase in fractal dimension and surface coverage ratio corresponds to reduced inter-tube tunneling distances and facilitated carrier hopping across CNT junctions. Consequently, electrical conductivity increased monotonically within the fractal dimension range of 1.84–1.88. At the same time, CNT-rich agglomerates act both as conductive nodes and localized scattering centers, influencing carrier mobility and energy distribution and thereby affecting thermoelectric response. The observed inverse relationship between Seebeck coefficient and electrical conductivity is consistent with carrier concentration effects and morphology-induced modulation of energy-dependent transport.

A direct correlation between surface roughness parameters (S_k, S_v, and S_z) and Seebeck coefficient further demonstrates that surface morphology is not merely a geometric descriptor but an active factor governing charge transport and entropy flow. TE characterization revealed a maximum Seebeck coefficient of 104 μV K^{-1} and a maximum PF of 0.0032 μW m^{-1} K^{-2}, confirming that functionalized SWCNT incorporation enhances charge transport under an applied thermal gradient.

Overall, the findings demonstrate that fractal dimension and statistical surface descriptors can serve as predictive structural parameters linking morphology to electrical and thermoelectric performance. Controlled morphological heterogeneity—arising from balanced CNT dispersion and limited agglomeration—emerges not as a processing imperfection but as a tunable design

variable for optimizing multifunctional CNT-reinforced polymer composites.

Funding

This study, carried out within the scope of the project coded 2024/082, was supported by Balıkesir University Scientific Research Projects Unit.

References

1. P. M. Ajayan, "Carbon Nanotubes: Novel Architecture in Nanometer Space," *Progress in Crystal Growth and Characterization of Materials* 34 (1997): 37, https://doi.org/10.1016/S0960-8974(97)00004-1.

2. M. Endo, T. Hayashi, Y. Ahm Kim, M. Terrones, and M. S. Dresselhaus, "Applications of Carbon Nanotubes in the Twenty–first Century," *Philosophical Transactions of the Royal Society A* 362 (2004): 2223, https://doi.org/10.1098/rsta.2004.1437.

3. A. Ilgaz, "Material Performance Characterization of Carbon Nanotubes and BYK, 8003 Organic Compounds Reinforced GFRP Composites," *European Physical Journal Applied Physics* 97, no. 10 (2022), https://doi.org/10.1051/epjap/2022210227.

4. B. R. Reddivari, S. Vadapalli, B. Sanduru, T. Buddi, K. M. Vafaeva, and A. Joshi, "Fabrication and Mechanical Properties of Hybrid Fibre-Reinforced Polymer Hybrid Composite with Graphene Nanoplatelets and Multiwalled Carbon Nanotubes," *Cogent Engineering* 11, no. 1 (2024): 2343586, https://doi.org/10.1080/23311916.2024.2343586.

5. A. Ilgaz and M. Bayırlı, "Fractal Characterization for Conductivity Mechanism of Single-Walled Carbon Nanotube Doped Composites," *Indian Journal of Physics* 98 (2024): 1335, https://doi.org/10.1007/s12648-023-02916-4.

6. O. B. Mergen, E. Umut, E. Arda, and S. A. Kara, "A Comparative Study on the AC/DC Conductivity, Dielectric and Optical Properties of Polystyrene/Graphene Nanoplatelets (PS/GNP) and Multi-Walled Carbon Nanotube (PS/MWCNT) Nanocomposites," *Polymer Testing* 90 (2020): 106682, https://doi.org/10.1016/j.polymertesting.2020.1066.

7. C. H. Sun, F. Li, Z. Ying, C. Liu, and H. Cheng, "Surface Fractal Dimension of Single-Walled Carbon Nanotubes," *Physical Review B* 69 (2004): 033404–033401, https://doi.org/10.1103/PhysRevB.69.033404.

8. A. Macías-García, M. A. Díaz-Díez, M. Alfaro-Domínguez, and J. P. Carrasco-Amador, "Influence of Chemical Composition, Porosity and Fractal Dimension on the Electrical Conductivity of Carbon Blacks," *Heliyon* 6 (2020): 04024, https://doi.org/10.1016/j.heliyon.2020.e04024.

9. A. Pander, T. Onishia, A. Hattaa, and H. Furuta, "Study of Self-Organized Structure in Carbon Nanotube Forest by Fractal Dimension and Lacunarity Analysis," *Materials Characterization* 160 (2020): 110086, https://doi.org/10.1016/j.matchar.2019.110086.

10. A. Ilgaz and M. Bayırlı, "Fractal Characterization of Polyester Based Standard and Single Walled Carbon Nanotube Modified Composites," *Zeitschrift für Naturforschung A* 78 (2023): 443, https://doi.org/10.1515/zna-2023-0029.

11. V. Shinde, M. Uthayakumar, and R. Karthick, "Self-Assembled Cobalt Hydroxide Micro Flowers from Nanopetals: Structural, Fractal Analysis and Molecular Docking Study," *Surfaces and Interfaces* 32 (2022): 102163, https://doi.org/10.1016/j.surfin.2022.102163.

12. N. Jia, J. Cao, X. Yi Tan, et al., "Thermoelectric Materials and Transport Physics," *Materials Today Physics* 21 (2021): 100519, https://doi.org/10.1016/j.mtphys.2021.100519.

13. A. Abd-Elsalam, H. O. Badr, A. A. Abdel-Rehim, and Iman S. El-Mahallawi, "Structure and Thermoelectric Behavior of Polyaniline-Based/CNT-Composite," *Current Applied Physics* 36 (2022): 88, https://doi.org/10.1016/j.cap.2021.11.012.

14. B. Dörling, S. Sandoval, P. Kanklaa, A. Fuertes, G. Tobias, and M. Campoy-Quiles, "Exploring Different Doping Mechanisms in Thermoelectric Polymer/Carbon Nanotube Composites," *Synthetic Metals* 225 (2017): 70, https://doi.org/10.1016/j.synthmet.2017.01.002.

15. C. A. Schneider, W. S. Rasband, and K. W. Eliceirive, "NIH Image to ImageJ: 25 Years of Image Analysis," *Nature Methods* 9 (2012): 671, https://doi.org/10.1038/nmeth.2089.

16. A. B. Schroeder, E. T. A. Dobson, C. T. Rueden, P. Tomancak, F. Jug, and KWEliceiri ve, "The ImageJ Ecosystem: Open-Source Software for Image Visualization, Processing, and Analysis," *Protein Science* 30 (2021): 234, https://doi.org/10.1002/pro.3993.

17. M. Zhang, W. Zhang, N. Jiang, D. N. Futaba, and M. Xu, "A General Strategy for Optimizing Composite Properties by Evaluating the Interfacial Surface Area of Dispersed Carbon Nanotubes by Fractal Dimension," *Carbon* 154 (2019): 457, https://doi.org/10.1016/j.carbon.2019.08.017.

18. H. Liu, Y. Zhang, and W. Huang, "Fractal Analysis of Surface Morphology in Polymer/CNT Gas Sensors and Its Influence on Sensitivity," *Surface and Interface Analysis* 53, no. 6 (2021): 421–591, https://doi.org/10.1002/sia.6945.

19. S. Ahmed, A. Kausar, and T. Iqbal, "Role of Surface Morphology in Carbon Nanotube-Polymer Nanocomposite Gas Sensors," *Journal of Nanomaterials* 2023 (2023): 1–12, https://doi.org/10.1155/2023/9954326.

20. R. Kumar, RSingh A.Rani, and M. Kumar, "Carbon Nanotube-Based Composite Materials for Gas Sensors: A Review," *Sensors and Actuators B: Chemical* 304 (2020): 127371, https://doi.org/10.1016/j.snb.2019.127371.

21. M. Kunduraci, D. Çirmi, S. D. Çalhan, and U. Çağlayan, "Significance of Surface Roughness in the Supercapacitor Activity of Nickel-Based Electrodes," *Applied Physics A* 127 (2021): 618, https://doi.org/10.1007/s00339-021-04784-3.

22. A. Feldhoff, "Thermoelectric Material Tensor Derived from the Onsager–de Groot–Callen Model," *Energy Harvesting and Systems* 2, no. 1-2 (2015), https://doi.org/10.1515/ehs-2014-0040.